ACS APPLIED MATERIALS & INTERFACES

www.acsami.org

Forum Article

Contactless Resolution of Inflammatory Signals in Tailored Macrophage-Based Cell Therapeutics

Ana F. Almeida, Margarida S. Miranda, Adriana Vinhas, Márcia T. Rodrigues,* and Manuela E. Gomes*

Cite This: https://doi.org/10.1021/acsami.2c22505

Read Online

ACCESS | Metrics & More | Article Recommendations | Supporting Information

ABSTRACT: In recent years, nanotechnology-based microRNA (miR) therapeutic platforms have shown great promise for immunotherapy and tissue regeneration, despite the unmet challenge of achieving efficient and safe delivery of miRs. The transport of miRs offers precision and regulatory value for a myriad of biological processes and pathways, including the control of macrophage (Mφ) functions and, consequently, the inflammatory cascades Mφ are involved in. Thus, enforcement of Mφ can boost the regenerative process and provide new solutions for diverse chronic pathologies. In this study, we sought to develop a magnetically guided transporter to deliver an miR-155 antagonist to M1-primed Mφ. Furthermore, we determined its modulatory effect in reprogramming Mφ from inflammatory to pro-regenerative phenotypes, with the aim of tissue healing and regenerative medicine approaches. This strategy combines contactless and high-precision control of Mφ, anticipating new functional miR carriers for targeted strategies controlled by extracorporeal action. The magnetoplexes SPION@PEI-miR were efficiently delivered into Mφ without compromising cell viability and successfully induced miR-mediated gene silencing by enhancing the expression of anti-inflammatory markers (IL4 and IL10) and the production of M2φ-related markers (CD206 and IL4). Given its multimodal features, SPION@PEI-miR represents a simple, safe, and nonviral theranostic platform that enables imaging, tracking, and miR delivery with modulatory effects on immune cells.

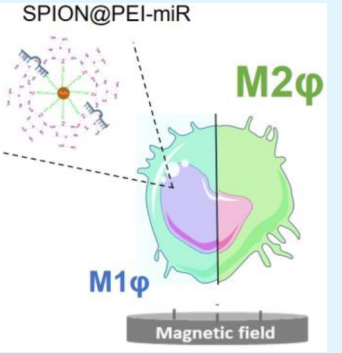

KEYWORDS: *miR-155, RNA delivery, macrophages, SPION, magnetoplexes*

INTRODUCTION

Recent understanding of the role and contribution of immune cells in disease onset and progression has motivated advances in the fields of immunotherapies and tissue regeneration. Macrophages (Mφ) play a significant role in immunological signaling and immune system control.[1] They serve as the initial line of defense and initiate sequentially coordinated inflammatory cascades that are necessary for effective tissue repair and regeneration. The plasticity of Mφ in response to external stimuli guides its inflammatory (M1φ) and regenerative (M2φ) phenotypes. Although M1 predominance is necessary to initiate inflammation after damage, if perpetuated in time, it can be harmful to tissue healing, disrupt physiological responses, and fail to control chronic inflammatory states.[2] Therefore, reprogramming Mφ functions to manage pro-inflammatory signals in later healing phases or in chronic inflammatory conditions provides alternative targeted therapies for a variety of lesions and inflammatory diseases.

MicroRNAs (miRs) can be highly important for the transition between different states of Mφ polarization. miRs are a group of small RNA species of approximately 21 to 23 nucleotides that control post-transcriptional gene expression by attaching to the 3′-untranslated region of their target mRNAs.[3] In contrast to siRNA, which affects a single gene, miR-targeted therapy can influence entire cellular pathways or activities, echoing the message without genetic imprinting or pharmaceutical drugs. Synthetic oligonucleotides can be used to supplement downregulated or nonfunctional miRs, whereas artificial antagonists, either oligonucleotides or small molecules, can block the effects of overexpressed miRs.[4] The Food and Drug Administration (FDA) approval of RNA-based molecules for the treatment of cancer and neurodegenerative and respiratory disorders has created opportunities for RNA exploitation as a new generation of nanotherapeutics with a targeted design for any gene with limited off-target effects. Diverse miR species including miR-21,[5,6] miR-146a,[7] miR-155,[8,9] and miR-223[10] have been shown to coordinate the changes in Mφ phenotypes. miR-155 in particular is inherently involved in M1φ polarization. Bone marrow-derived murine Mφ deficient in miR-155 express lower levels of pro-inflammatory cytokines,[11,12] similar to miR-155-lacking RAW264.7 Mφ[13] and human Mφ with silenced miR-155.[14] Additionally, it has been demonstrated that miR-155 stimulation prevents M2φ polarization by interfering with the translation of several molecules in the interleukin-13 and 4

Special Issue: Materials and Interfaces in Regenerative Medicine

Received: December 14, 2022
Accepted: July 20, 2023

(IL13/IL4) pathway.[15] These findings suggest that miR-155 is likely a master switch in inflammation and the start of repair programs in Mφ, making it an appealing target for therapeutic intervention.

The development of safe and efficient carriers is the greatest challenge in miR-guided therapies. The molecular weight, hydrophilic character, and negative charge of miR molecules result in poor cell membrane permeability.[16] When administered intravenously, miRs can be rapidly degraded by enzymes, leading to restricted trafficking, off-target effects, and limited efficiency.

Magnetically assisted technologies offer versatile nanotransporters with multimodal properties to ensure miR bioavailability to Mφ directly or upon local or systemic administration. Magnetic nanomaterials, such as superparamagnetic iron oxide nanoparticles (SPION), have been clinically used as magnetic resonance imaging (MRI) contrast agents for decades[17] and constitute a research hotspot for DNA and RNA carriers because of their easy surface modification and magnetic navigation for contactless control, *in vivo* trafficking, and real-time monitoring, with a very low tendency to form particle aggregates after external magnetic field (EMF) removal, which favors *in vivo* compatibility[18,19] and distribution at precise locations. Moreover, improved internalization of both permissive and reluctant transfection cell lines was successfully achieved with SPION-based nanoparticles[20] using magnetofection. Supporting the high cell penetration achieved by magnetofection, Rohiwal et al. integrated SPION with polyethylenimine (PEI) and reported an efficient nanotransporter to mediate the nonviral CRISPR-Cas9 method for gene editing.[21] SPION were coated with positively charged PEI and CRISPR-Cas9 plasmid-forming magnetoplexes, which were successfully transferred into HEK 293-TLE-3 cells by actuation of an EMF.[21]

Despite these promising results, studies on RNA-loaded complexes focusing on nonintegrative gene strategies that address miRs are scarce.[22,23] This is likely due to the limited knowledge on how miR is used in the cell and to the well-established viral and nonviral transfection methods including exosomes,[24,25] and different types of nanoparticles (e.g., liposomes and micelles).[26,27] However, these methods present limitations, as exosomes are technically challenging and may transport unwanted RNA species, liposomes may interfere with cell membranes and induce *in vivo* toxicity, and nanoparticles often lack proper *in vivo* distribution, which jeopardizes efficiency outcomes. Additionally, most of these studies were cancer-oriented[28,29] with unique M1/M2 dynamics, which are unsuitable for treating chronic inflammatory profiles. The precise tuning regulation in space and time makes miRs an excellent candidate class for new immunoregulatory perspectives to transiently target and shut down desirable gene expression using cell-free therapies. Moreover, targeting and guiding immune cell responses that reinforce self-resolving inflammation can dramatically ameliorate chronic inflammation.

Therefore, in the present study, we propose to design a magnetically responsive miR-loaded nanotransporter (magnetoplex) that enables imaging, tracking, and miR delivery with modulatory action on immune cells to guide the phenotypic transition of M1-primed Mφ via magnetofection.

The magnetoplex will transport an miR-155-5p antagonist for the inhibition of overexpressed miR-155, attenuating the synthesis and prevalence of pro-inflammatory mediators and anticipating the blossom of anti-inflammatory signaling. To our knowledge and despite the nanocarriers developed in the past few years, none have integrated contactless and high-precision control of Mφ mediated by miR regulation, foreseeing targeted strategies with theranostic potential controlled by extracorporeal action. Intracellular delivery of miRs is also expected to overcome the extracellular barriers and phagocytosis mechanisms associated with the M1φ function.

The successful guidance of Mφ, which naturally pursues inflammatory environments and regulates immune signaling, contributes to innovative platforms for the control of Mφ function by using miR-guided therapy. Our approach anticipates a cell-oriented alternative to nanocarriers to overcome the hurdles for RNA delivery and to balance the ratio of pro-inflammatory and pro-regenerative functional states of Mφ.

MATERIALS AND METHODS

Synthesis and Characterization of SPION@PEI and SPION@PEI-miR. *Preparation of SPION Coated with PEI (SPION@PEI).* SPION@PEI was prepared by coating commercial SPION functionalized with carboxylic acid groups (SPION-COOH) with branched polyethylenimine (PEI) through electrostatic interactions. Initially, the iron (Fe) concentration of commercial SPION-COOH (747254, Sigma-Aldrich, St. Louis, USA) was determined using inductively coupled plasma-optical emission spectroscopy (ICP-OES). The nanoparticles were digested with nitric acid (HNO_3) at 65 °C for 1 h. The solution was then cooled to room temperature (RT) and subsequently diluted with ultrapure water to a HNO_3 concentration of 5%. A calibration curve was constructed before the sample analysis using eight standard samples containing 0−10 mg/L Fe. Standard solutions were prepared by diluting an Fe standard solution (1000 mg/L Fe in 5% HNO_3) with ultrapure water. The wavelength used for the Fe determination was 259.94 nm. Measurements were performed using a Horiba Jobin Yvon, Inc., ICP spectrometer model JY 2000 2. To prepare SPION@PEI, SPION-COOH and PEI (MW 10 000 Da, 40331, Thermo Scientific, Ward Hill, USA) were diluted in sodium chloride (NaCl) (Sigma-Aldrich, St. Louis, USA). Different NaCl solutions (10, 50, and 100 mM) were tested for the coating process, of which the 50 mM solution was the most suitable for coating SPION-COOH with PEI. Then, SPION-COOH was added dropwise to PEI at three Fe:PEI mass ratios of 1:3, 1:10, and 1:17, and the resultant mixtures were agitated overnight. PEI-coated SPION with different Fe:PEI mass ratios were collected by centrifugation at 2500 × g in an ultrafiltration tube (Amicon Ultra-2 Centrifugal Filter Unit, MW cutoff of 100 kDa, Merck, Darmstadt, Germany). A borate buffer (20 mM, Merck, Darmstadt, Germany) pH 7.4 was used during the purification washing steps because it was suitable for maintaining a low polydispersity index (PDI) of the magnetic nanoparticles during the purification process. Four washing steps were performed until PEI was undetectable in the supernatant. To evaluate the efficacy of the purification process, the concentration of amine groups in the initial supernatant and washing supernatants was determined using 2,4,6-trinitrobenzenesulfonic acid (TNBS) (Sigma-Aldrich, St. Louis, USA), as described previously.[30] The supernatants were dissolved in a 0.1 M borate buffer (pH 9.3). A volume of 2.5 μL of a freshly prepared TNBS solution (0.03 M) was added to 100 μL of the supernatants. After 30 min of agitation to ensure complete mixing, the absorbance was measured using a UV−vis spectrophotometer at 420 nm (Synergy HT, BioTek, Winooski, USA). The concentration of PEI was calculated using a calibration curve derived from PEI solutions with concentrations of 0.5, 0.25, 0.1, 0.05, and 0 mg/mL prepared in 0.1 M borate buffer (pH 9.3) (Supporting Information, Table S1). For subsequent use in biological studies, the Fe concentrations of SPION@PEI 1:3, 1:10, and 1:17 were determined by ICP-OES, as previously described.

Preparation of SPION@PEI Conjugated with FITC (SPION@PEI(FITC)). To analyze the presence of the magnetic nanoparticles in

https://doi.org/10.1021/acsami.2c22505
ACS Appl. Mater. Interfaces XXXX, XXX, XXX−XXX

macrophages, SPION@PEI(FITC) was produced by conjugating PEI with fluorescein isothiocyanate (FITC). The synthesis of PEI(FITC) was based on the reaction between the primary amino group of PEI and the isothiocyanate group of FITC (≥90%, Sigma-Aldrich, St. Louis, USA). FITC (10 mg/mL) dissolved in dimethyl sulfoxide (DMSO) (ACS reagent, 99.9%, Sigma-Aldrich, St. Louis, USA) was slowly added to a PEI solution (10 mg/mL) prepared in 0.1 M sodium bicarbonate buffer (pH 9.2). The resulting mixture was continuously stirred for 1 h at RT in the dark. The solution was then dialyzed in a dialysis membrane (MW cutoff 5 kDa) against distilled water for 3 days with frequent water changes. The coating of SPION-COOH with PEI(FITC) was performed as previously described for coating SPION-COOH with PEI.

Preparation of miR Solution and Fabrication of SPION@PEI-miR Complexes. For miR delivery into cells, the produced SPION@PEI was bonded to the miR via electrostatic interactions to form a magnetic complex (SPION@PEI-miR). The synthetic miR antagonist hsa-miR-155-5p (HSTUD0254, Sigma-Aldrich, St. Louis, USA) was diluted with RNase-free water (Thermo Scientific, Ward Hill, USA) to a final concentration of 10 μM. The same procedure was followed for the synthetic miR antagonist control (NCSTUD001, Sigma-Aldrich, St. Louis, USA), which was exclusively used for characterization purposes.

For the biological experiments, SPION@PEI (1:3) at the concentration of 2.2 μg Fe/mL was loaded with a miR cargo of 0.05 and 0.15 μg miR (SPION@PEI-miR[0.05] and SPION@PEI-miR[0.15], respectively). For that, after a 30 min sterilization under ultraviolet radiation, SPION@PEI were 30 min incubated with 0.05 or 0.15 μg of miR-155 antagonist at RT to allow the formation of the SPION@PEI-miR magnetoplex. The mature sequences of the synthetic miRs HSTUD0254 and NCSTUD001 are included in the Supporting Information (Table S2).

Physicochemical Characterization. The hydrodynamic size, polydispersity index (PDI), and zeta potential of SPION@PEI and SPION@PEI-miR were determined using a Malvern NanoZS instrument (Malvern Instruments, Malvern, UK). The stability of these systems was evaluated by measuring their size and zeta potential as a function of time (7 days). The elemental compositions of SPION@PEI and SPION@PEI-miR were determined by energy-dispersive X-ray spectroscopy (EDX) (INCAx-Act, PentaFET Precision, Oxford Instruments, Abingdon, UK).

Binding Ability of miR to SPION@PEI. To analyze the binding efficiency of miR to SPION@PEI, different Fe:miR mass ratios were tested by using agarose gel electrophoresis. RNase-free microcentrifuge tubes were filled with 2 μL of synthetic miR antagonist control (NCSTUD00, Sigma-Aldrich, St. Louis, USA) (±0.15 μg of miR/tube). Next, increasing amounts of Fe of SPION@PEI (0; 0.015; 0.075; 0.15; 0.22; 0.30 and 0.75 μg) were added to the tubes. The mixture was incubated at RT for 30 min to allow the formation of the SPION@PEI-miR complex. During this period, a 3% agarose gel was prepared by dissolving agarose (Seakem LE agarose, Lonza Bioscience, Rockland, USA) in 1× Tris-borate-EDTA buffer (Sigma-Aldrich, St. Louis, USA). A 2 μL portion of 6× TriTrack DNA Loading Dye (Thermo Scientific, Vilnius, Lithuania) was added to each sample, and the total sample volume was adjusted to 20 μL using RNase-free water (Thermo Scientific, Ward Hill, USA). All samples were loaded into the gel, and electrophoresis was performed at 100 V/cm (EPS 301 Power Supply, Ge Healthcare, Uppsala, Sweden) until the samples migrated to two-thirds of the length of the gel. The gel was stained with SYBR Safe DNA gel stain solution (Thermo Scientific, Carlsbad, USA) for 30 min using an agitator and visualized using the Odyssey Fc Imaging System 2800 (LI-COR, Inc., Lincoln, USA). A control well containing only miR (referred to as "Naked miR") was included in the gel run. The Fe:miR mass ratios at which miR forms complexes with SPION@PEI should not present bands representing free miR. Following the manufacturer's instructions, a Quant-iT RiboGreenTM RNA Assay Kit (Thermo Scientific, Bleiswijk, The Netherlands) was used to quantify the free miR present in the supernatants of SPION@PEI-miR after brief centrifugation. Sample fluorescence was measured at 480/520 nm using a Synergy HT microplate reader (BioTek, Winooski, USA).

Intracellular Delivery Studies of SPION@PEI with Magnetically Assisted Technologies. Human monocytes (THP1) American Type Culture Collection (ATCC): TIB-202 were cultured in Roswell Park Memorial Institute Medium (RPMI) (Sigma-Aldrich, St. Louis, USA) supplemented with 1% L-glutamine (Thermo Scientific, Bleiswijk, Netherlands) and 10% fetal bovine serum (FBS) (Thermo Scientific, Carlsbad, USA) in a humidified 5% CO_2 atmosphere. THP1 monocytes were differentiated into macrophages (Mφ) using phorbol 12-myristate 13-acetate (PMA) (100 nM, Sigma-Aldrich, St. Louis, USA) and further cultured and expanded in RPMI medium. For *in vitro* polarization studies with SPIONS@PEI-miR, cells were further incubated with 20 ng/mL interferon-gamma (IFN-γ) (Peprotech, Rocky Hill, USA) and 100 ng/mL lipopolysaccharide (LPS) (Sigma-Aldrich, St. Louis, USA) for classical macrophage activation (M1φ).

MTS Assay for Cytotoxicity Assessment of SPION@PEI at Different Ratios. Following cells seeding on 96-well plates (Corning Inc., Corning, USA) (1×10^5 cells/well) and PMA differentiation, various concentrations of SPION@PEI (0−8.8 μg/mL) at different mass ratios (1:3, 1:10, 1:17) were added to the cells, and magnetofection was provided by a magnefect nano device (nanoTherics Ltd., Warrington, UK) (350 mT/well). After the respective time points (day 1 or day 4), cytotoxicity was determined by [3-(4, 5-dimethylthiazol-2-yl)-5-(3-carboxymethoxyphenyl)-2-(4-sulfophenyl)-2 H-tetrazolium (MTS dye, 5:1 ratio, Promega, Madison, USA) uptake at 490 nm using a Synergy HT microplate reader (BioTek, Winooski, USA).

Testing the Influence of Different Magnetic Fields on Magnetofection. Mφ was seeded on 96-well plates (1×10^5 cells/well) and PMA differentiated before the administration of different concentrations of SPION@PEI(FITC) (2.2 to 52.8 μg/mL). Magnetofection was provided for 20 min by (i) a static magnetic field (SMF) using a magnefect nano device (nanoTherics Ltd., Warrington, UK) (350 mT/well) or (ii) a pulsed electromagnetic field (PEMF) of 100 G, 60 Hz, 0.05% duty cycle using a magnetotherapy device (Magnum XL Pro, Globus Corporation, Codognè, Italy). The supernatant of the cells (culture medium) was analyzed for the magnetofection efficiency. The fluorescence signal of the FITC tag in the SPION@PEI(FITC) complexes remaining in the supernatant was read using a microplate reader (485/528 nm, Synergy HT, BioTek, Winooski, USA). For colocalization purposes, cells were marked with CellTracker CM-DiI Dye (Thermo Scientific, Carlsbad, USA) for 40 min at 37 °C, followed by a 10 min incubation at RT with 4,6-Diamidino-2-phenyindole (DAPI) (1:1000, Thermo Scientific, Carlsbad, USA) and visualized by confocal laser scanning microscopy (TCS SP8, Leica Mannheim, Germany). 3D reconstruction images were obtained from z-stacks using TCS SP8 software (Leica, Mannheim, Germany).

***In Vitro* Polarization Studies.** After cells were seeded in 96-well plates (1×10^5 cells/well) and differentiated (M1φ-primed) as described in the previous section, two time points (day 1 or day 4) and four conditions were investigated. Thus, M1φ were cultured with (i) SPION@PEI-miR (0.05 or 0.15 μg/mL), (ii) miR-free SPION@PEI, (iii) Naked miR (0.15 μg/mL), and (iv) untreated M1φ (termed M1-primed Mφ). Condition (ii) was used as an experimental control for miR functionalization, while condition (iii) was used as a control for the delivery efficiency of the magnetoplexes. Condition (iv) enables the assessment of the magnetic stimulation on cell responses in the absence of the system. The SMF magnetofection was performed as described in the previous sections. During M1φ treatment under different conditions, RPMI without FBS supplementation was used to avoid possible interference with miR activity.

Viability Evaluation of M1φ Treated with the SPION@PEI-miR Complexes. Cell proliferation was evaluated using a Deep Blue Cell Viability (Alamar Blue) kit (BioLegend, San Diego, USA). M1φ were washed with PBS and incubated with a 10% solution of deep-blue cell viability in the dark for 4 h at 37 °C. The supernatants were then collected and the fluorescence signal was acquired at 530/590 nm

https://doi.org/10.1021/acsami.2c22505
ACS Appl. Mater. Interfaces XXXX, XXX, XXX−XXX

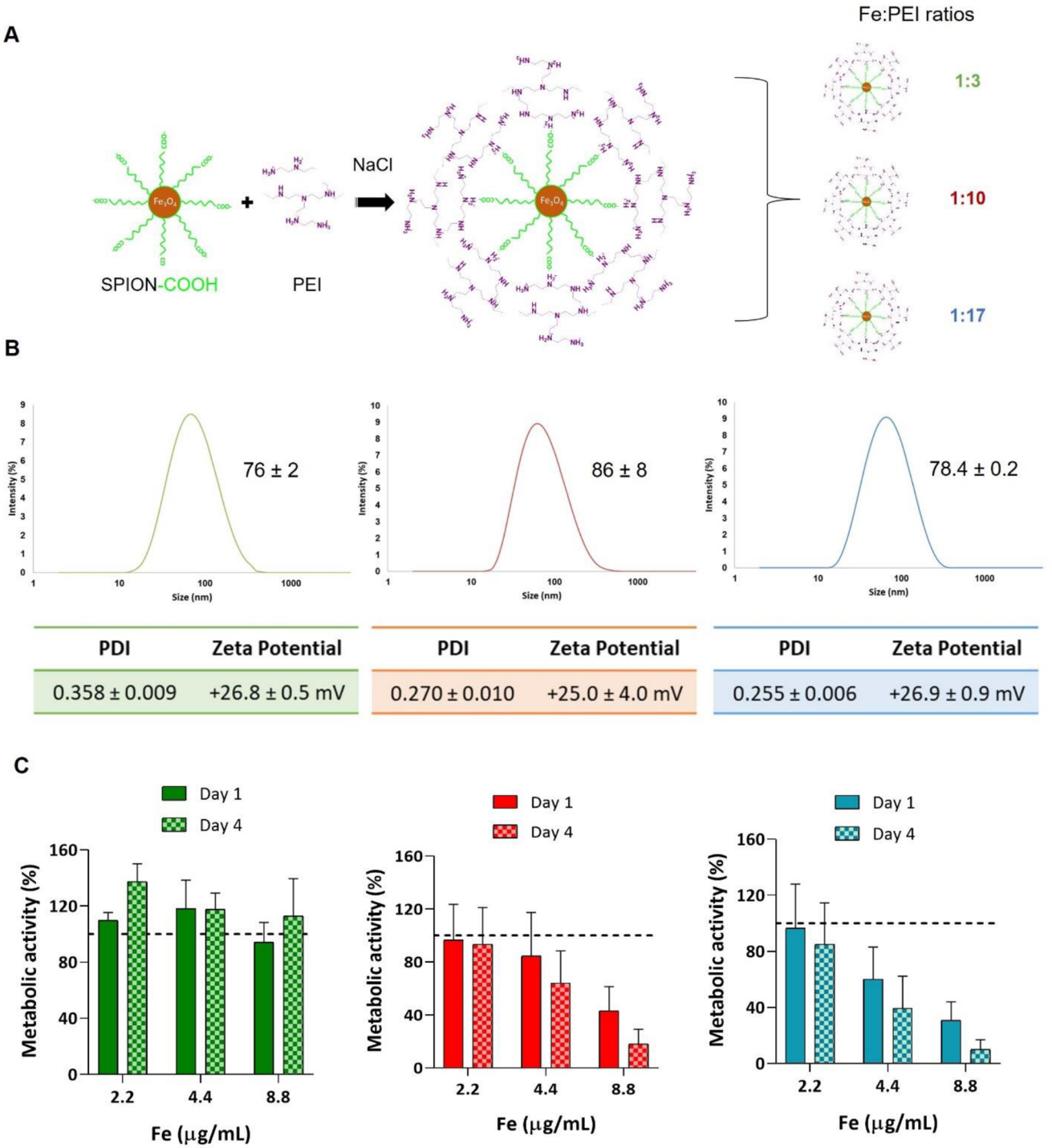

Figure 1. Synthesis, characterization, and cytotoxicity assessment of SPION@PEI with different Fe:PEI mass ratios. (A) Schematic representation of the SPION coating with PEI at 1:3 (green), 1:10 (red), and 1:17 (blue) iron (Fe):PEI mass ratios. (B) Hydrodynamic size distribution and surface charge of SPION@PEI and (C) cell metabolic activity assessed by MTS assay in macrophages (Mφ) cultured for 1 or 4 days with different concentrations of SPION@PEI (2.2 to 8.8 μg/mL). The graph bars represent the mean ± standard error of the mean (SE) of three independent experiments.

using a Synergy HT microplate reader (BioTek, Winooski, USA). Live/dead cell double staining: M1φ were washed with PBS and incubated in the dark with 2 μM calcein AM in PBS (Thermo Scientific, St. Louis, USA) and 4 μM propidium iodide (Thermo Scientific, St. Louis, USA) for 30 min at 37 °C. The cells were rinsed in PBS, and the fluorescence signal was acquired using an Upright Microscope with Thunder (DM6 B, Leica, Mannheim, Germany).

Morphological Features of M1φ after Exposure to SPION@PEI-miR Magnetoplexes. Scanning electron microscopy (SEM) (JEOL, Tokyo, Japan) was used to visualize and acquire images of the morphological features of M1φ 4 days after exposure to the SPION@PEI-miR complexes. Following the respective treatments, M1φ was fixed in 4% neutral buffered formalin (Thermo Scientific, Kalamazoo, USA) overnight and dehydrated using ascending concentrations of ethanol (from 30 to 100%), followed by a 5 min immersion in

https://doi.org/10.1021/acsami.2c22505
ACS Appl. Mater. Interfaces XXXX, XXX, XXX−XXX

hexamethyldisiloxane (HMSO) (Sigma-Aldrich, St. Louis, USA). The samples were air-dried overnight and sputter-coated (30 s at 20 mA, C5219, Model 108A, Cressington, UK) with gold.

RNA Isolation and Gene Expression Analysis. Gene expression analysis provides important insights into Mφ differentiation and polarization. *IL4* and *IL10* are well recognized negative regulators, whereas *IL8* and *TNFα* are documented as positive regulators of pro-inflammatory responses in Mφ. The balance between these two categories of molecules contributes to homeostasis being important to measure the levels of both to identify Mφ functional states. Total RNA was extracted using TRIzol Reagent (Thermo Scientific, Carlsbad, USA) following the manufacturer's instructions. The RNA was quantified using a Nanodrop ND-1000 spectrophotometer (Thermo Scientific, Carlsbad, USA) at 260/280 nm. First-strand complementary DNA was synthesized from 1 μg of RNA from each sample (qScriptTM cDNA Synthesis Kit, Quanta Biosciences, Gaithersburg, USA) in a 20 μL reaction using a Mastercycler ep realplex gradient S machine (Eppendorf, Hamburg, Germany). Transcripts were quantified by quantitative polymerase chain reaction (qPCR) using the PerfeCTA SYBR Green FastMix kit (Quanta Biosciences, Gaithersburg, USA) following the manufacturer's protocol in a Real-Time Mastercycler ep realplex thermocycler (Eppendorf, Hamburg, Germany). Primer sequences (Supporting Information, Table S3) were designed using Primer 3 software. The 2−ΔΔCt method was used to evaluate the relative expression level of each target gene.[31] An untreated condition (M1-primed Mφ) was used to determine the relative expression, and the transcript expression of target genes (*IL4, IL10, IL8*, and *TNFα*) was normalized to that of the endogenous housekeeping gene Tyrosine 3-Monooxygenase/Tryptophan 5-Monooxygenase Activation Protein Zeta (YWHAZ). Normalization of gene expression values was also performed against Naked miR.

Cell Internalization and M2φ-Related Marker Studies by Flow Cytometry. The effects of SMF and PEMF on the cellular internalization of magnetoplexes were evaluated by flow cytometry using FTIC-labeled magnetoplexes (SPION@PEI(FITC)). A range of 0−52.8 μg/mL of magnetoplexes (iron content) was investigated in cells as previously described in the Section "Testing the Influence of Different Magnetic Fields on Magnetofection".

Mφ was identified and gated using forward and side scattering. A minimum of 10,000 cells were acquired using a BD FACSCalibur flow cytometer (BD Biosciences, Erembodegem-Aalst, Belgium) and analyzed using Cell Quest software. Unstained cells (0 μg/mL) were used to establish the cell autofluorescence. A nonmagnetic condition was also assessed as an experimental control. The Mφ population that was positive for FITC was expressed as a percentage.

The number of cells positive for IL4 ($IL4^+$) and CD206 ($CD206^+$) was also determined to characterize the Mφ phenotypes. For this, Mφ were incubated with Anti-IL4 antibody [8D4−8] (Phycoerythrin) (ab95717, Abcam, Cambridge, UK) and FITC Mouse Anti-Human CD206 (551135, BD Biosciences, Környe, Hungary) for 30 min. Cells were then washed with PBS and resuspended in acquisition buffer (1% formaldehyde in PBS) before acquisition on a FACSAria III sorter equipped with blue and red lasers (BD Biosciences, Erembodegem-Aalst, Belgium). Cells were identified by forward and side scatter. A minimum of 5000 cells were acquired and analyzed using the FACS Diva software version 7. Unstained cells were used to establish cell autofluorescence. The population of positive cells was expressed in percentage values. Representative histograms from day 4 are available in the Supporting Information, Figure S4.

Detection of IL10. The detection of IL10 in the culture media was assessed using an enzyme-linked immunoassay (ELISA) kit (R&D systems, Minnesota, EUA), according to the manufacturer's instructions.

Detecting Patterns of Cytokine Expression. The cocktail of cytokines/chemokines released by Mφ is part of the molecular communication involved in inflammatory signaling and is indispensable for characterizing Mφ polarization. Having this in mind, after the respective time points, supernatants were collected and analyzed using a Human Cytokine Array C1 (RayBiotech Life Inc., Peachtree Corners, USA) following the manufacturer's instructions. This array simultaneously detects the expression levels of diverse anti-inflammatory (CCL7 and CCL2) and pro- inflammatory (IL8, CCL5, CCL8, CXCL1, and CXCL9) molecules, whose spot intensities can be further measured. The spot intensity was detected using an Odyssey Fc Imaging System 2800 (LI-COR Inc., Lincoln, USA) and quantified using LI-COR acquisition Image Studio software, version 5.2.5.

Data Analysis. The results are expressed as the mean ± standard error of the mean (SE), representative of three independent experiments ($n = 3$) analyzed in duplicate, except for the flow cytometry experiments, which are representative of two independent experiments ($n = 2$). Statistical analysis was performed using SPSS statistical software (version 27.0.1.0). First, a Shapiro-Wilk test was used to ascertain data normality and Levene's test for homogeneity of variances. Normality and variance homogeneity were rejected, and nonparametric tests were used (Kruskal−Wallis test followed by Tukey's HSD test). Different degrees of confidence were considered: $p < 0.05$, $p < 0.01$, $p < 0.001$, and $p < 0.0001$, and are represented by the symbols * for $p < 0.05$, ** for $p < 0.01$, *** for $p < 0.001$, and **** for $p < 0.0001$.

RESULTS AND DISCUSSION

SPION@PEI Synthesis and Characterization. In this study, we modified the surface of SPION with the synthetic cationic polymer polyethylenimine (PEI) (branched form, 10 kDa molecular weight) (SPION@PEI) (Figure 1A) because of its ability to electrostatically interact with the negatively charged phosphate groups of miR, thus enabling the formation of stable SPION-miR complexes. PEI-based methods are considered the gold standard for transfection procedures because of PEI's high nucleic acid complexation efficiency and distinctive buffering effect on lysosomal escape.[32] Moreover, PEI-based formulations have been employed as safe nonviral vectors for gene delivery[33] as well as DNA vaccines.[34,35]

We selected branched PEI because of its additional advantages over linear PEI, providing primary, secondary, and tertiary amino groups that more effectively bind nucleic acids, whereas low-molecular-weight PEI lowers the cytotoxic potential of the system.[36] Furthermore, the modification of SPION with PEI molecules increases the nucleic acid transfection efficiency of PEI alone, as magnetic-based systems can be internalized in cells under the guidance of an EMF via magnetofection.

We investigated different solutions for optimizing SPION@PEI binding, including water and different concentrations of sodium chloride (NaCl, 10−100 mM). However, all of the solutions investigated, except for the 50 mM NaCl solution, led to particle aggregation (data not shown), which compromised the formation of SPION@PEI with the appropriate size and a uniform size distribution. Since dimension control is highly relevant for small molecule binding, such as miR species and cellular internalization, 50 mM was selected to produce our nanovehicles.

Three iron (Fe):PEI mass ratios of 1:3, 1:10, and 1:17 were explored to determine the most adequate PEI coating for binding, stabilizing, and carrying miR species. The SPION@PEI formulations presented monodisperse hydrodynamic diameters in the range of 76−86 nm, as assessed by dynamic light scattering (Figure 1B). Independent of the Fe:PEI mass ratio, the surface charge of SPION@PEI was approximately +26 mV (Figure 1B), reflecting the presence of amine moieties in PEI, conferring the ability to bind electrostatically to negatively charged miRs. SPION@PEI was stable in an aqueous solution for at least 30 days. SPION@PEI presented

https://doi.org/10.1021/acsami.2c22505
ACS Appl. Mater. Interfaces XXXX, XXX, XXX−XXX

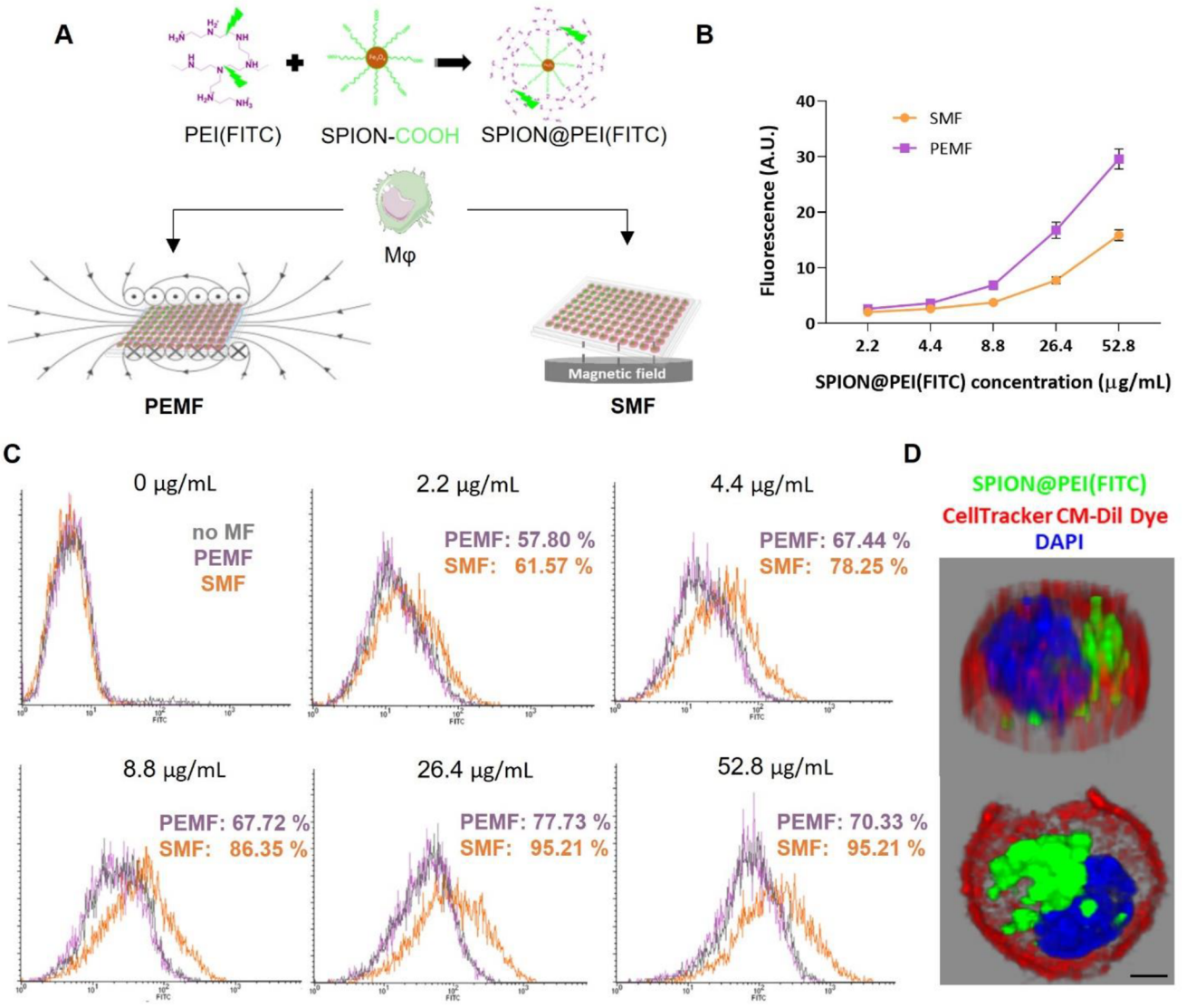

Figure 2. Magnetofection efficiency by applying different magnetic field methods. (A) Schematic representation of the magnetofection procedures using FITC-tagged SPION@PEI (SPION@PEI(FITC)) and Mφ stimulated by static (SMF − 350 mT/well, 20 min) or dynamic (PEMF − 100 G, 60 Hz, 0.05% duty cycle, 20 min) magnetic fields. (B) Quantification of the fluorescence signal in the medium of Mφ, previously cultured with SPION@PEI(FITC) (2.2−52.8 μg/mL) and upon 20 min of stimulation with SMF or PEMF. (C) Flow cytometry analysis for the identification of SPION@PEI(FITC) taken up by Mφ 24 h after SMF or PEMF stimulation. (D) 3D reconstructed images representative of the colocalization of SPION@PEI(FITC) with a particle concentration of 4.4 μg/mL (green) in Mφ (CellTracker CM-Dil Dye, red) after SMF stimulation. Mφ nuclei were counterstained with DAPI (blue). Scale bar: 5 μm.

a narrow size distribution and a positive surface charge at physiological pH, which are favorable features for the effective binding of oligonucleotides to SPION. These results also suggest that the amount of PEI in the Fe:PEI mass ratio did not significantly contribute to increasing the dimensions or influencing the surface charge of the nanoparticles. The presence of PEI in SPION@PEI was further confirmed by Fourier-transform infrared spectroscopy (FTIR), owing to the detection of peaks assigned to the stretching and bending of the −CH2− groups and the N−H bending vibration from the amine moieties present in PEI (Supporting Information, Figure S1).

The cytotoxic potential associated with the electrostatic interaction of PEI with the cell membrane[37] was investigated by measuring the metabolic activity of Mφ in the three Fe:PEI mass ratios (Figure 1C) in function of the nanoparticle concentrations (2.2 μg/mL, 4.4 μg/mL, and 8.8 μg/mL). The nanoparticle concentration was determined by quantifying Fe using ICP-OES. The metabolic activity of Mφ was influenced by the Fe concentration, especially at ratios of 1:10 and 1:17, indicating increased values even at lower Fe concentrations. The highest percentage of metabolically active cells was observed at a 1:3 mass ratio without significant differences among nanoparticle concentrations.

Considering the physicochemical outcomes and biocompatibility of the SPION@PEI formulations, an Fe:PEI 1:3 mass ratio was chosen for further cell culture assays.

Tackling Intracellular Delivery of SPION@PEI upon Application of Different Magnetic Fields. External magnetic fields (EMFs) have been shown to assist in the uptake of various biomolecules with improved transfection efficiencies.[38] Most research on magnetofection employs static

https://doi.org/10.1021/acsami.2c22505
ACS Appl. Mater. Interfaces XXXX, XXX, XXX−XXX

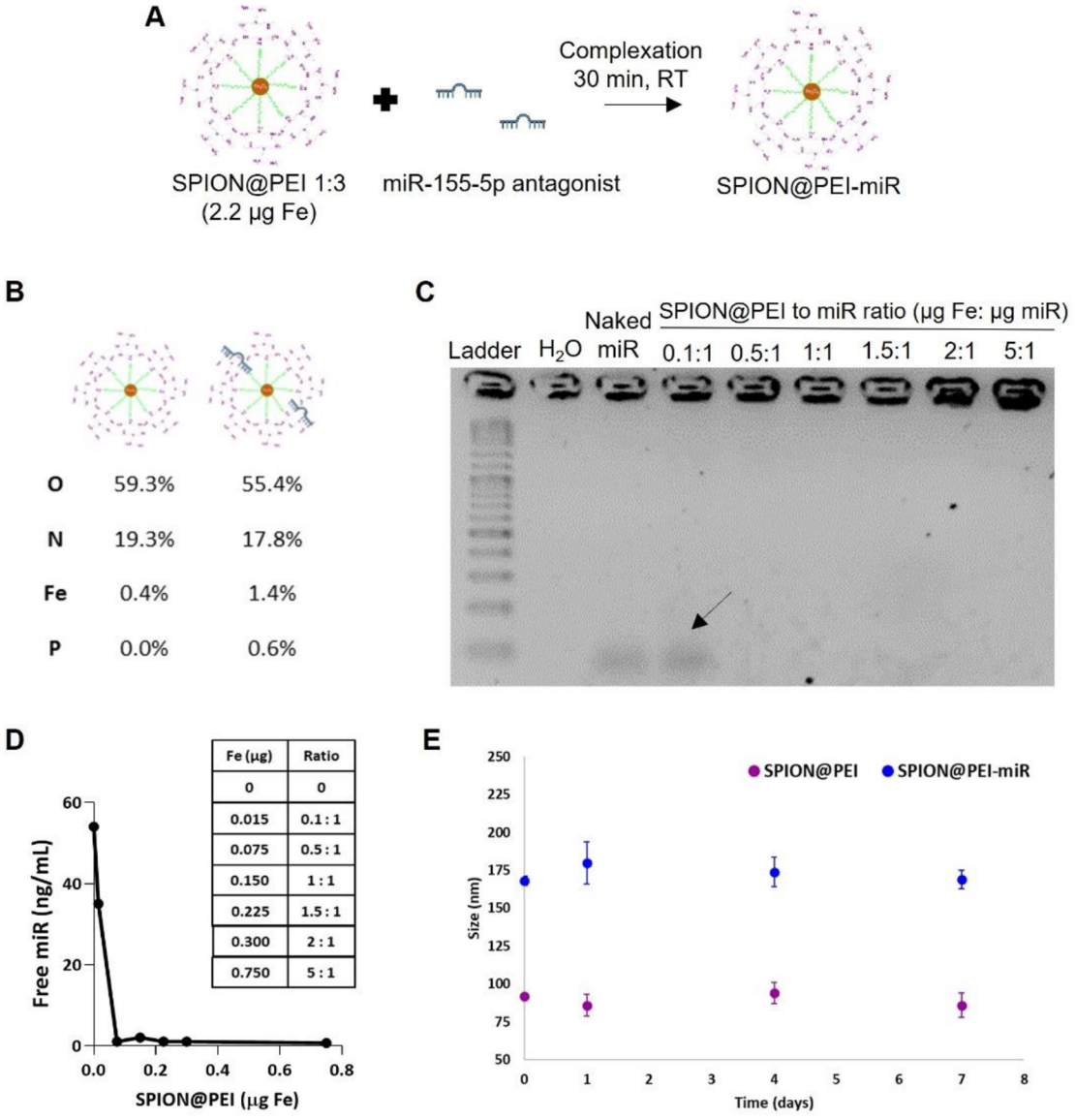

Figure 3. Electrostatic binding of SPION@PEI-miR and SPION@PEI-miR characterization. (A) Schematic representation of SPION@PEI−miR production. (B) EDX analysis of the SPION@PEI and SPION@PEI-miR complexes represented by the percentages of oxygen (O), nitrogen (N), iron (Fe), and phosphorus (P) quantified in these complexes. (C) Agarose gel electrophoresis of SPION@PEI-miR with different Fe:miR mass ratios (μg/μg, 0.1:1 to 5:1). (D) Free miR quantification using a Ribogreen kit to assess the binding capability of miR to SPION@PEI. Naked miR represents free miR. The table indicates the iron content (μg) present at each Fe:miR ratio studied. (E) Dimensions of SPION@PEI-miR and SPION@PEI as a function of time in a 5:1 ratio (Fe:miR). The charge stability over time is presented in the Supporting Information (Figure S3).

magnetic fields (SMFs) produced by rare-earth magnets, typically neodymium−iron-boron magnets.[39] SMFs enable efficient cell uptake, avoiding cell membrane interactions in a relatively simple and fast procedure.[40] However, it has been demonstrated that pulsed electromagnetic fields (PEMFs) preserve the benefits of magnetofection while introducing oscillatory movements on the cell surface that appear to boost the internalization efficiency.[41]

The magnetic responsiveness of magnetoplexes can be affected by the iron content of particles.[40] Thus, to clarify the macrophage uptake of SPION@PEI upon the actuation of different EMFs (SMF vs PEMF) a 20 min actuation was investigated (Figure 2A) using a wider range of particle concentrations, namely, 0−52.8 μg/mL (Figure 2B and 2C) (instead of 0−8.8 μg/mL as shown in Figure 1). The EMF parameters were selected based on the promising outcomes of previous studies.[42−44] For imaging purposes, SPION@PEI was tagged with fluorescein isothiocyanate (FITC) (SPION@PEI(FITC)) via the reaction of the primary amines of PEI with the isothiocyanate group of FITC.

Higher fluorescence intensity was observed in the culture medium collected from PEMF-stimulated Mφ, corresponding to noninternalized SPION@PEI(FITC). The high-intensity signal of extracellular particles suggests reduced particle uptake and, consequently, low internalization efficiency compared to SMF-stimulated Mφ (Figure 2B). Supporting these outcomes, the number of cells with internalized SPION@PEI(FITC) was higher in the SMF (orange) than in the PEMF (purple) or nonmagnetic (gray) conditions (Figure 2C). This tendency is not influenced by the particle concentration and supports the applicability of SMF as a standard magnetically assisted transfection method. Although PEMF has shown clinical

https://doi.org/10.1021/acsami.2c22505
ACS Appl. Mater. Interfaces XXXX, XXX, XXX−XXX

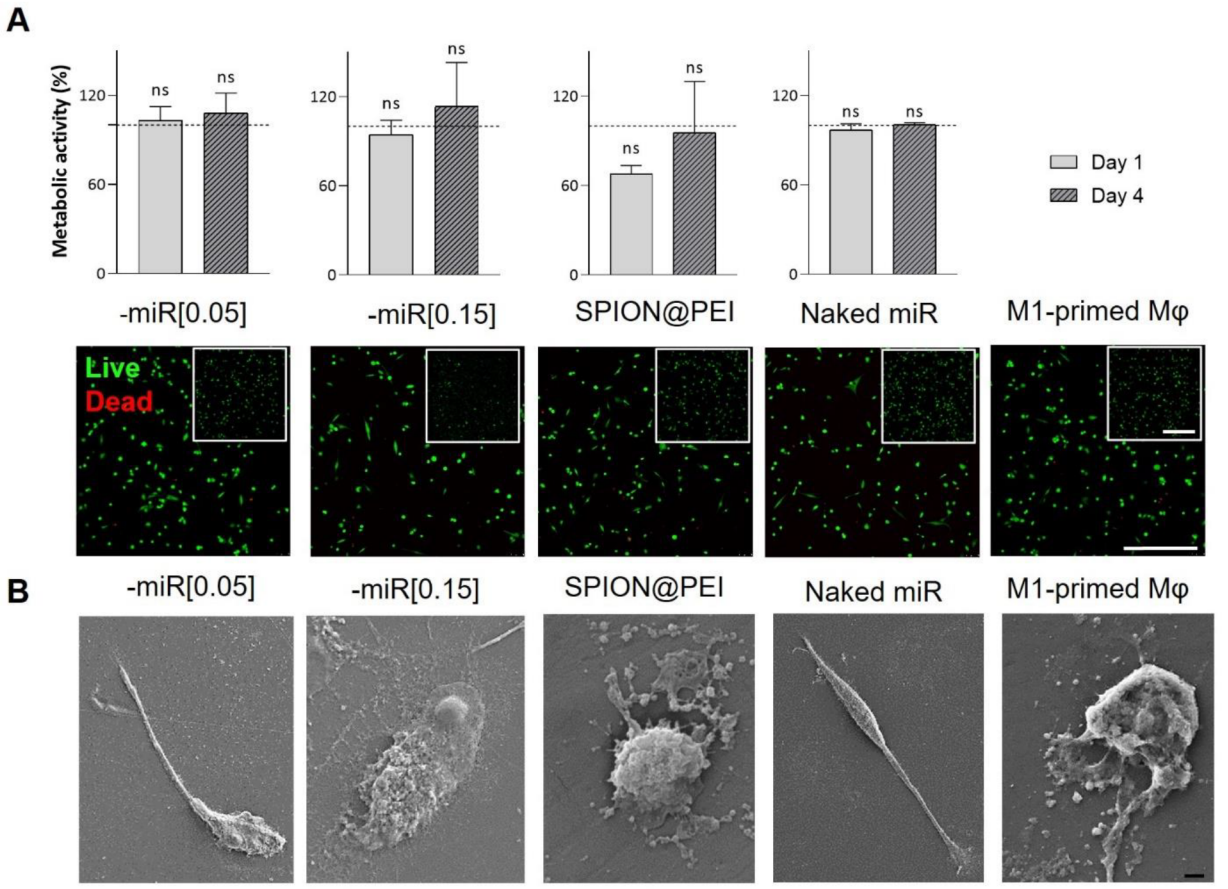

Figure 4. Viability and morphological characterization of M1-primed Mφ after SPION@PEI-miR delivery. (A) Top: Alamar Blue metabolic activity assay. Cell metabolic activity was quantified by normalizing the reduced Alamar Blue values to those of the M1-primed Mφ, which were considered 100% and are represented in the graphs by the horizontal dotted line. Bottom: Representative images of the live/dead assay performed with Calcein AM-labeled (live, green) and propidium iodide-labeled (dead, red) 1 day (inset) and 4 days after SPION@PEI-miR delivery. Scale bar = 50 μm. (B) SEM micrographs of Mφ morphological features 4 days after delivery. Scale bar = 2 μm. Naked miR represents M1-primed Mφ supplemented with the free SPION@PEI-free mir-155 antagonist (no SPION@PEI). The graph bars represent the mean ± SE of three independent experiments.

therapeutic potential, SMF is more efficient in facilitating magnetically responsive uptake. The 3D reconstruction of z-stack fluorescent images also showed the colocalization of SPION@PEI(FITC) within Mφ (Figure 2D), indicating effective internalization by static magnetofection. Consistently, images of Mφ stained with Perl's blue (Supporting Information, Figure S2) also revealed higher iron accumulation (blue spots) from SPION@PEI(FITC) in SMF-stimulated cells at all particle concentrations assessed.

These results are in accordance with the literature[42] on improved cellular uptake by SMF-responsive systems, suggesting the applicability of SPION@PEI as a potential carrier for intracellular delivery.

Assembly and Characterization of SPION@PEI-miR Magnetoplexes. After the selection of the SPION@PEI formulation (Fe:PEI; 1:3 mass ratio), the most promising method for magnetic stimulation (SMF), and the lowest nanoparticle concentration (2.2 μg/mL, iron content) for effective and biocompatible magnetoplex production, SPION@PEI was electrostatically conjugated with a miR-155 antagonist (SPION@PEI-miR) (Figure 3A). By conjugating the miR-155 antagonist to SPION@PEI, we expected to attenuate the expression of pro-inflammatory molecules in M1-primed Mφ and stimulate anti-inflammatory mediators whose expression is downregulated under inflammatory conditions.

Energy dispersive spectroscopy (EDX) analysis confirmed the existence of miR on the surface of SPION@PEI, as indicated by the presence of phosphorus (P) in the elemental mapping (%P = 0.6 in comparison to miR-free SPION@PEI: %P = 0.0; Figure 3B). To visualize the miR-binding capability of SPION@PEI, different Fe:miR mass ratios of SPION@PEI-miR complexes were subjected to agarose gel electrophoresis (Figure 3C). When binding to magnetoplexes occurs, naturally negatively charged miR molecules do not travel through the gel and the band corresponding to the molecular weight of miR is not detectable. The analysis revealed that beyond the 0.5:1 mass ratio the free miR band was not visualized, implying a successful bond between the miR and SPION@PEI, indicating 100% miR binding efficiency. To support these results, the miR concentrations in the supernatants were investigated using spectroscopy (Figure 3D). As expected, the amount of free miR decreased to values close to zero at a 0.5:1 mass ratio, corroborating the electrophoresis results.

The size of SPION@PEI-miR increased relative to that of SPION@PEI owing to the complexation with miR (7.6 kDa) (Figure 3E). In addition, the negative charge of the miR

https://doi.org/10.1021/acsami.2c22505
ACS Appl. Mater. Interfaces XXXX, XXX, XXX−XXX

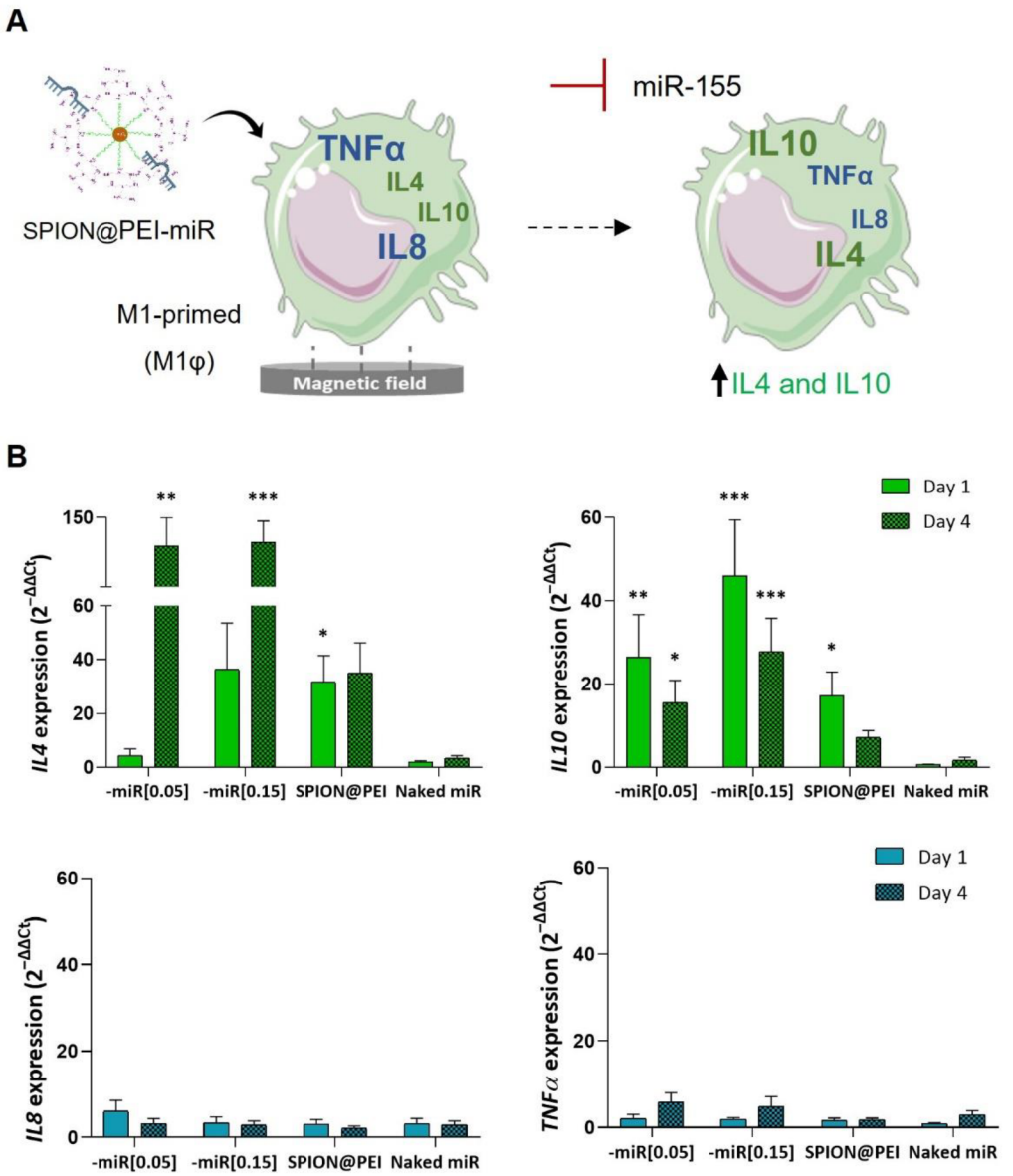

Figure 5. miR-mediated polarization of macrophages. (A) Scheme of the strategy assessing the efficiency of SPION@PEI-miR to block miR-155 action. (B) Relative expression levels of anti-inflammatory (IL4 and IL10) and pro-inflammatory (IL8 and TNFα) markers established by qPCR calculated with the $-\Delta\Delta$Cp method 1 or 4 days after magnetoplex delivery to the cells. Statistical evaluation was performed using the Kruskal–Wallis test, followed by Tukey's HSD test. Significance values: * $p < 0.05$, ** $p < 0.01$, *** $p < 0.001$ compared to cells supplemented with Naked miR. Legend: SPION@PEI: miR-free magnetoplexes; SPION@PEI-miR[0.05]: magnetoplexes loaded with 0.05 μg of miR-155 antagonist; SPION@PEI-miR[0.15]: magnetoplexes loaded with 0.15 μg of miR-155 antagonist; Naked miR: M1-primed Mφ supplemented with free miR-155 antagonist. The graph bars represent mean ± SE of three independent experiments.

influenced the zeta potential of SPION@PEI-miR, indicating slightly decreased values relative to miR-free magnetoplexes (Figure S3 in the Supporting Information). Both systems showed univariable/steady values over time in an aqueous solution (Figure 3E and Figure S3), indicating their stability at physiological pH. These results support a flexible temporal window that allows for the transportation of small instructive molecules in body fluids and their biodistribution to hard-to-reach tissues or organs. Altogether, these results confirm that SPION@PEI electrostatically binds miR and that the binding is strong enough to conjugate small concentrations of miR.

Viability and Morphological Features of Mφ. Reports on the effective dosage of miR cargo are scarce and depend on multiple parameters, including animal model, cell type, mRNA targets, and administration routes.[45] Thus, we produced SPION@PEI-miR with two concentrations of miR-155 antagonist (0.05 or 0.15 μg/mL, SPION@PEI-miR[0.05] and SPION@PEI-miR[0.15], respectively) to reduce the inflammatory cues in M1-primed Mφ. The same mass of iron related to the 1:3 SPION:PEI ratio was used for both miR concentrations as well as a particle concentration of 2.2 μg/mL (iron content). Our reasoning was that if a specific amount of iron was bonded to 0.15 μg of miR, a lower amount of miR (0.05 μg) would also be bonded to that same specific amount of iron, yet leaving free binding sites.

Metabolic activity was determined using Alamar Blue (Figure 4A, top) and live/dead (Figure 4A, bottom) assays 1 and 4 days after magnetofection. As expected, miR cargos did

https://doi.org/10.1021/acsami.2c22505
ACS Appl. Mater. Interfaces XXXX, XXX, XXX−XXX

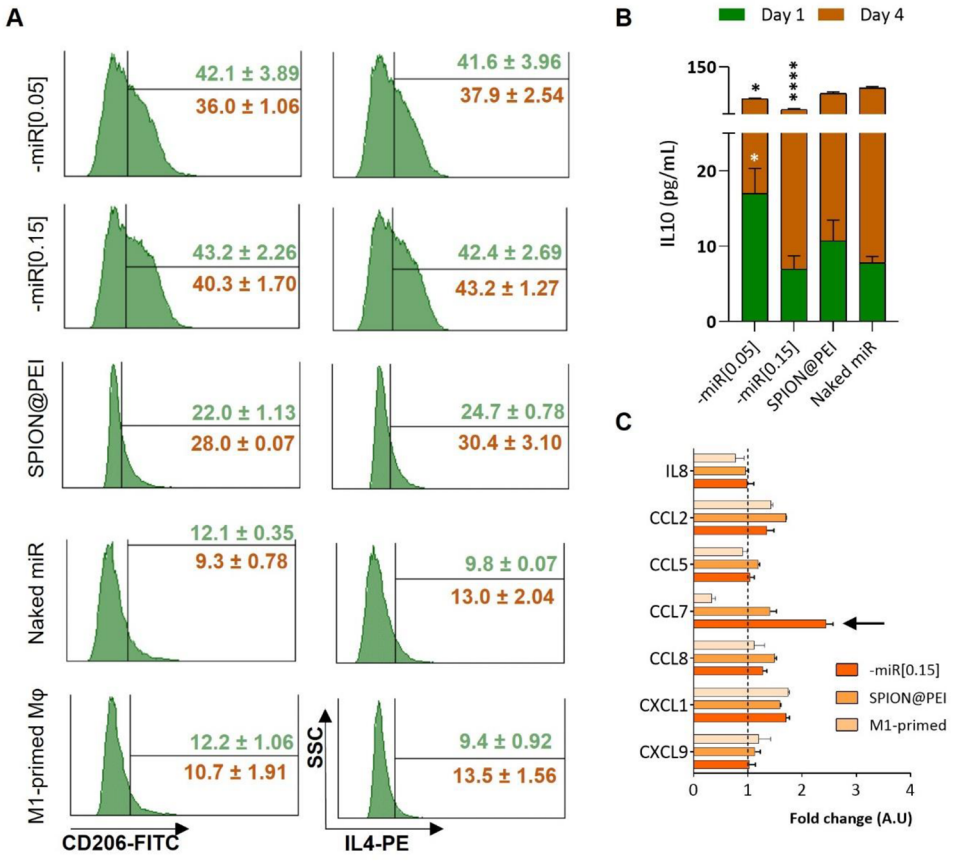

Figure 6. Macrophages' protein signature after SPION@PEI-miR treatment. (A) Representative flow cytometry histograms indicating the percentage of $CD206^+$ FITC (left) and $IL4^+$ PE (right) Mφ on day 1 (green) or day 4 (orange) after magnetoplex or Naked miR delivery. The histograms are related to day 1. Day 4 histograms are shown in the Supporting Information, Figure S4. (B) Detection of IL10 using ELISA. Statistical evaluation was performed using the Kruskal–Wallis test followed by Tukey's HSD test. Significance values: * $p < 0.05$, **** $p < 0.0001$ compared with cells supplemented with Naked miR. (C) Reactivity of the proteome arrays in M1-primed Mφ 4-days after delivery of SPION@PEI, SPION@PEI-miR, or Naked miR. Naked miR was considered as the reference array (represented by the vertical dotted line). Photographs of the membranes are shown in Supporting Information, Figure S5.

not cause toxic effects, thus proving to be suitable concentrations for cell-based approaches. Nevertheless, 4 days after SPION@PEI-miR delivery, the cell metabolic activity slightly increased (Figure 4A, top). Literature reports that Mφ polarization entails metabolic reprogramming, in which M1φ displays reduced levels of oxidative phosphorylation (OXPHOS) and fatty acid oxidation (FAO), whereas M2φ is characterized by enhanced OXPHOS and FAO.[46] Considering that Alamar Blue is a redox activity indicator, these results may indicate an immunomodulatory time-course effect of SPION@PEI-miR on Mφ.

Scanning electron microscopy (SEM) analysis revealed healthy cells that tended to acquire an elongated form with miR-loaded magnetoplexes, also supporting the occurrence of phenotypic immune modulation (Figure 4B) and in line with existing morphological data for different Mφ subsets, associating M2φ with stretched and elongated morphology.[47,48]

Impact of SPION@PEI-miR on the Inflammatory Profile of M1-Primed Mφ. Targeting a single mediator of inflammation has shown limited effectiveness in modulating Mφ behavior and surpassing the redundant mechanisms of inflammatory responses. Therefore, the use of miRs to control the transcription of sets of inflammation-related genes is an attractive therapeutic option.

Approaching a miR antagonist strategy, we investigated the efficiency of SPION@PEI-miR to block miR-155 action in the synthesis of inflammatory cytokines of M1-primed Mφ (Figure 5A). THP1-derived Mφ was stimulated with lipopolysaccharide (LPS) and interferon gamma (IFNγ) for 24 h, followed by magnetofection with SPION@PEI-miR complexes.

As shown in Figure 5B, the delivery of SPION@PEI-miR to M1-primed Mφ led to a significant upregulation in interleukins 4 and −10 (IL4 and IL10, respectively). The levels of IL4 were significantly increased 4 days after miR delivery, independent of the miR concentration used ([0.05]: $p < 0.01$ and [0.15]: $p < 0.001$, in comparison to the Naked miR condition), but there was a tendency for gene expression enhancement with increasing miR concentrations.

As a powerful anti-inflammatory cytokine, IL4, is critically involved in the pathways associated with M2φ responses.[49] A higher percentage of Mφ expressed the protein form of IL4 after miR delivery (Figure 6A and Supporting Information, Figure S4), demonstrating the successful inhibition of miR-155 and miR-mediated repolarization of Mφ functions with magnetoplexes.

Like IL4, IL10 is an anti-inflammatory cytokine that attenuates multiple inflammatory processes. A significant increase was observed for IL10 at both time points, especially after delivery with the -miR[0.15] load ([0.15]: $p < 0.001$ in

https://doi.org/10.1021/acsami.2c22505
ACS Appl. Mater. Interfaces XXXX, XXX, XXX−XXX

comparison to Naked miR) (Figure 5B). IL10 has been shown to inhibit miR-155 in response to LPS in a signal transducer and activator of transcription 3 (STAT3)-dependent manner,[50] while miR-155 decreases IL10 production.[14] The increase in IL10 expression suggests an effective blockage of miR-155 function. Moreover, the increased expression of both IL4 and IL10, combined with miR-loaded magnetoplexes, indicates a synergistic interaction that enhances M2φ differentiation.[51] The inflammatory mediators interleukin-8 (IL8) and tumor necrosis factor α (TNFα) were also analyzed using quantitative polymerase chain reaction (qPCR). No significant differences were detected in the expression of these genes ($p > 0.05$) when compared to cells supplemented with the Naked miR-155 antagonist. The low expression of IL8 and TNFα also indicates the inhibition of miR-155 and, consequently, restrained expression of inflammatory genes favoring the M2φ phenotype.

Strikingly, miR-free SPION@PEI also influenced the early translation of IL4 and IL10 ($p < 0.05$, compared to Naked miR, day 1) (Figure 5B). Although the induced gene expression was lower than that resulting from the miR-loaded magnetoplexes, this suggests anti-inflammatory action of the system itself. These results are interesting because the data available on SPION-based systems in this matter are controversial. Several studies have reported that PEI-coated SPION can activate M1φ,[52] whereas others seem to support our findings.[53] Not only were IL10 and IL4 increased, but the expression of IL8 and TNFα was also reduced. Consequently, our vehicles can contribute to regulatory actions to minimize the exacerbated responses of Mφ in inflammatory niches, establishing their potential feasibility in strategies aimed at preventing persistent inflammatory triggers and chronic inflammation.

Previous *in vitro* studies have reported that IL4-induced M2φ enhances the production of mannose receptor (CD206).[54] Therefore, we analyzed the percentage of CD206$^+$ Mφ (Figure 6A). Consistent with the literature, Mφ treated with SPION@PEI-miR complexes showed increased numbers of IL4$^+$/CD206$^+$ Mφ. The miR concentration (0.05 and 0.15 μg/mL) does not influence the number of IL4$^+$/CD206$^+$ Mφ, which is around 4× higher than that in M1-primed Mφ populations.

We further investigated the detection of IL10 using ELISA after treatment with magnetoplexes (Figure 6B). IL10 was produced in all SPION@PEI formulations, with increased amounts in SPION@PEI-miR[0.05] ($p = 0.0335$). The miR[0.05] effect seems to be more evident in a short time (day 1), which may be relevant to stimulating specific mediators or activating certain inflammatory pathways, thus reinforcing the pro-regenerative action of the particles. In summary, the SPION@PEI-miR formulation encouraged the expression of several M2 markers, including CD206, IL4, and IL10 supporting its anti-inflammatory and pro-regenerative action.

Although we did not observe an miR-concentration dependency for the inflammation-related markers studied, the SPION@PEI-miR[0.15] formulation was investigated to screen the protein forms of inflammatory mediators using an antibody array system. The miR[0.15] load is directly comparable to the Naked miR condition, in which M1-primed Mφ was supplemented with 0.15 μM of naked miR-155 antagonist.

Chemokines are a family of small cytokines that regulate circulation, homing, and retention of immune cells.[55] Unlike most of the screened proteins, which showed basal levels and similar amounts under all conditions, chemokine (C−C motif) ligand 7 (CCL7) showed high levels of secretion (Figure 6C and Supporting Information, Figure S5). CCL7 mediates the recruitment of immune cells to reduce inflammation by binding to its receptors[56] and restricts the amount of local inflammation in mouse models.[57] The secreted form of CCL7 increased in the Naked miR and SPION@PEI conditions, but the highest values were detected in SPION@PEI-miR, assisting the biofunctionality of magnetoplexes addressing a constrained pro-inflammatory response.

The detection of pro-inflammatory chemokines (e.g., IL8, chemokine (C−C motif) ligands 5 and 8 (CCL5 and CCL8), chemokine (C-X-C motif) ligands 1 and 9 (CXCL1 and CXCL9)) even at low amounts, 4 days after miR delivery, provides evidence that inflammatory mediators are not completely shut down with miR-155 modulation and M2 stimulation. These results support the continuum of Mφ polarization states and suggest that chemokines participate in regulatory processes during the transitional stages.

CONCLUSIONS

In this study, we developed magnetically responsive inflammation-instructed nanocomplexes for the transport and delivery of an miR-155 antagonist.

We used magnetofection as a magnetically assisted technique for the intracellular delivery of nucleic acids in a plasmid-free manner. The miR coating and final charge of SPION@PEI-miR prevent the direct contact of PEI with external environments and consequently reduce the PEI-cell membrane interactions. Beyond the system assembly, the contribution of PEI for transfection purposes is considerably inferior to the magnetic field stimulus for all of the particle concentrations investigated. This is because of the intrinsic magnetic responsiveness of SPION in general and their superparamagnetic nature, which are key features for achieving an improved efficiency.

The design and production of the SPION@PEI systems was shown to play an important role in the noninflammatory properties of the vehicle. The selection of SPION, optimization of the iron/PEI ratios, and purification steps are likely to contribute to these outcomes. By controlling the size, charge, and coating efficiency of SPION@PEI, inflammatory mechanisms such as phagocytosis or the disturbance/interaction with the cellular membranes may be minimized, as well as Mφ signaling generating pro-inflammatory responses.

SPION@PEI transporters are recognized as anti-inflammatory vehicles, are well-tolerated by Mφ, and can successfully carry an miR load. Although Mφ responses were not miR-concentration-dependent, which may be explained by the complexity behind miR transcriptional signals and lack of reports on miR functional concentrations, 0.05 μg/mL produced significant biological effects on M2 markers expression. The miR-loaded system was more efficient than Naked miR supplementation, even at lower concentrations. Moreover, unlike conventional pharmacological agents, our systems offer low yet effective and safer dosages of nanotherapeutics and high precision combined with imaging and extracorporeal control.

https://doi.org/10.1021/acsami.2c22505
ACS Appl. Mater. Interfaces XXXX, XXX, XXX−XXX

This study strongly encourages further exploitation of miR carriers, aiming at a precise and spatiotemporally controlled trigger for M1/M2 switching, foreseeing applications in healing and tissue regeneration, immunotherapy, and bioengineering clinical solutions.

One of the limitations of this study was the lack of an *in vivo* assessment of magnetoplexes. This was partly because of the difficulty in defining functional miR concentrations to meet relevant local inflammation models with an efficient window of therapeutic action, which will be pursued in future studies. Nevertheless, the promising *in vitro* outcomes of miR-mediated modulation using a transient gene-silencing strategy to control inflammatory signaling create new opportunities for Mφ-based therapies and miR-guided treatment using SPION-based shuttles as a robust nanoplatform with high theranostic value.

■ ASSOCIATED CONTENT

Supporting Information

The Supporting Information is available free of charge at https://pubs.acs.org/doi/10.1021/acsami.2c22505.

Results related to the SPION@PEI characterization, Perl's blue staining for visualizing iron content, flow cytometry histograms, miR-155 antagonist mature sequences, and the primers used for the RT-qPCR analysis; Figure S1, FTIR spectrum of SPION and SPION@PEI; Figure S2, Perl's blue staining; Figure S3, zeta potential of SPION@PEI and SPION@PEI-miR as a function of time; Figure S4, representative flow cytometry histograms (day 4); Figure S5, photographs of the proteome arrays in M1-primed Mφ (day 4); Table S1, initial concentration of PEI for coating SPION-COOH (1:3) and the concentration of PEI in the discarded supernatant after purification; Table S2, mature sequences of miR antagonist hsa-miR-155-5p and miR antagonist control; Table S3, primers used for real time quantitative RT-qPCR analysis (PDF)

■ AUTHOR INFORMATION

Corresponding Authors

Márcia T. Rodrigues − *3B's Research Group, I3Bs − Research Institute on Biomaterials, Biodegradables and Biomimetics, University of Minho, Headquarters of the European Institute of Excellence on Tissue Engineering and Regenerative Medicine, Guimarães 4805-017, Portugal; ICVS/3B's−PT Government Associate Laboratory, Guimarães 4710-057, Portugal;* orcid.org/0000-0002-4483-5689; Phone: +351 253 510 913; Email: mrodrigues@i3bs.uminho.pt

Manuela E. Gomes − *3B's Research Group, I3Bs − Research Institute on Biomaterials, Biodegradables and Biomimetics, University of Minho, Headquarters of the European Institute of Excellence on Tissue Engineering and Regenerative Medicine, Guimarães 4805-017, Portugal; ICVS/3B's−PT Government Associate Laboratory, Guimarães 4710-057, Portugal;* orcid.org/0000-0002-2036-6291; Phone: +351 253 510 904; Email: megomes@i3bs.uminho.pt

Authors

Ana F. Almeida − *3B's Research Group, I3Bs − Research Institute on Biomaterials, Biodegradables and Biomimetics, University of Minho, Headquarters of the European Institute of Excellence on Tissue Engineering and Regenerative Medicine, Guimarães 4805-017, Portugal; ICVS/3B's−PT Government Associate Laboratory, Guimarães 4710-057, Portugal*

Margarida S. Miranda − *3B's Research Group, I3Bs − Research Institute on Biomaterials, Biodegradables and Biomimetics, University of Minho, Headquarters of the European Institute of Excellence on Tissue Engineering and Regenerative Medicine, Guimarães 4805-017, Portugal; ICVS/3B's−PT Government Associate Laboratory, Guimarães 4710-057, Portugal;* orcid.org/0000-0001-7633-8890

Adriana Vinhas − *3B's Research Group, I3Bs − Research Institute on Biomaterials, Biodegradables and Biomimetics, University of Minho, Headquarters of the European Institute of Excellence on Tissue Engineering and Regenerative Medicine, Guimarães 4805-017, Portugal; ICVS/3B's−PT Government Associate Laboratory, Guimarães 4710-057, Portugal*

Complete contact information is available at: https://pubs.acs.org/10.1021/acsami.2c22505

Notes

The authors declare no competing financial interest.

■ ACKNOWLEDGMENTS

This research was funded by the European Research Council, Consolidator Grant MagTendon, grant number 772817 and by the FCT - Fundação para a Ciência e a Tecnologia, scholarship number SFRD/BD/144816/2019.

■ REFERENCES

(1) Arango Duque, G.; Descoteaux, A., Macrophage Cytokines: Involvement in Immunity and Infectious Diseases. *Front. Immunol.* **2014**, *5*, DOI: 10.3389/fimmu.2014.00491.

(2) Atri, C.; Guerfali, F. Z.; Laouini, D. Role of Human Macrophage Polarization in Inflammation during Infectious Diseases. *Int. J. Mol. Sci.* **2018**, *19* (6), 1801.

(3) O'Neill, L. A.; Sheedy, F. J.; McCoy, C. E. MicroRNAs: the Fine-tuners of Toll-like Receptor Signalling. *Nature reviews. Immunology* **2011**, *11* (3), 163−75.

(4) Baumann, V.; Winkler, J. miRNA-based Therapies: Strategies and Delivery Platforms for Oligonucleotide and Non-oligonucleotide Agents. *Future medicinal chemistry* **2014**, *6* (17), 1967−84.

(5) Bejerano, T.; Etzion, S.; Elyagon, S.; Etzion, Y.; Cohen, S. Nanoparticle Delivery of miRNA-21 Mimic to Cardiac Macrophages Improves Myocardial Remodeling after Myocardial Infarction. *Nano Lett.* **2018**, *18* (9), 5885−5891.

(6) Wang, S. Y.; Kim, H.; Kwak, G.; Jo, S. D.; Cho, D.; Yang, Y.; Kwon, I. C.; Jeong, J. H.; Kim, S. H. Development of microRNA-21 mimic Nanocarriers for the Treatment of Cutaneous Wounds. *Theranostics* **2020**, *10* (7), 3240−3253.

(7) Bobba, C. M.; Fei, Q.; Shukla, V.; Lee, H.; Patel, P.; Putman, R. K.; Spitzer, C.; Tsai, M.; Wewers, M. D.; Lee, R. J.; et al. Nanoparticle Delivery of microRNA-146a Regulates Mechanotransduction in Lung Macrophages and Mitigates Injury During Mechanical Ventilation. *Nat. Commun.* **2021**, *12* (1), 289.

(8) Cai, X.; Yin, Y.; Li, N.; Zhu, D.; Zhang, J.; Zhang, C.-Y.; Zen, K. Re-polarization of Tumor-associated Macrophages to Pro-inflammatory M1Macrophages by microRNA-155. *Journal of Molecular Cell Biology* **2012**, *4* (5), 341−343.

(9) Jia, C.; Chen, H.; Wei, M.; Chen, X.; Zhang, Y.; Cao, L.; Yuan, P.; Wang, F.; Yang, G.; Ma, J. Gold Nanoparticle-based miR155 Antagonist Macrophage Delivery Restores the Cardiac Function in

Ovariectomized Diabetic Mouse Model. *International journal of nanomedicine* **2017**, *12*, 4963−4979.
(10) Saleh, B.; Dhaliwal, H. K.; Portillo-Lara, R.; Shirzaei Sani, E.; Abdi, R.; Amiji, M. M.; Annabi, N. Local Immunomodulation Using an Adhesive Hydrogel Loaded with miRNA-Laden Nanoparticles Promotes Wound Healing. *Small (Weinheim an der Bergstrasse, Germany)* **2019**, *15* (36), No. e1902232.
(11) Yu, F.; Jia, X.; Du, F.; Wang, J.; Wang, Y.; Ai, W.; Fan, D. miR-155-deficient Bone Marrow Promotes Tumor Metastasis. *Molecular cancer research: MCR* **2013**, *11* (8), 923−36.
(12) Nazari-Jahantigh, M.; Wei, Y.; Noels, H.; Akhtar, S.; Zhou, Z.; Koenen, R. R.; Heyll, K.; Gremse, F.; Kiessling, F.; Grommes, J.; Weber, C.; Schober, A. MicroRNA-155 Promotes Atherosclerosis by Repressing Bcl6 in Macrophages. *J. Clin. Invest.* **2012**, *122* (11), 4190−4202.
(13) Ma, Y. L.; Ma, Z. J.; Wang, M.; Liao, M. Y.; Yao, R.; Liao, Y. H. MicroRNA-155 Induces Differentiation of RAW264.7 Cells into Dendritic-like Cells. *Int. J. Clin. Exp. Pathol.* **2015**, *8* (11), 14050−14062.
(14) Kurowska-Stolarska, M.; Alivernini, S.; Ballantine, L. E.; Asquith, D. L.; Millar, N. L.; Gilchrist, D. S.; Reilly, J.; Ierna, M.; Fraser, A. R.; Stolarski, B.; McSharry, C.; Hueber, A. J.; Baxter, D.; Hunter, J.; Gay, S.; Liew, F. Y.; McInnes, I. B. MicroRNA-155 as a Proinflammatory Regulator in Clinical and Experimental Arthritis. *Proc. Natl. Acad. Sci. U. S. A.* **2011**, *108* (27), 11193−11198.
(15) Mahesh, G.; Biswas, R. MicroRNA-155: A Master Regulator of Inflammation. *Journal of Interferon Cytokine Research* **2019**, *39* (6), 321−330.
(16) Segal, M.; Slack, F. J. Challenges Identifying Efficacious miRNA Therapeutics for Cancer. *Expert Opinion on Drug Discovery* **2020**, *15* (9), 987−991.
(17) Dulińska-Litewka, J.; Łazarczyk, A.; Hałubiec, P.; Szafrański, O.; Karnas, K.; Karewicz, A. Superparamagnetic Iron Oxide Nanoparticles-Current and Prospective Medical Applications. *Materials (Basel, Switzerland)* **2019**, *12* (4), 617.
(18) Kandasamy, G.; Maity, D. Recent Advances in Superparamagnetic Iron Oxide Nanoparticles (SPIONs) for In Vitro and In Vivo Cancer Nanotheranostics. *Int. J. Pharm.* **2015**, *496* (2), 191−218.
(19) Miranda, M. S.; Almeida, A. F.; Gomes, M. E.; Rodrigues, M. T. Magnetic Micellar Nanovehicles: Prospects of Multifunctional Hybrid Systems for Precision Theranostics. *Int. J. Mol. Sci.* **2022**, *23* (19), 11793.
(20) Balcells, L.; Fornaguera, C.; Brugada-Vilà, P.; Guerra-Rebollo, M.; Meca-Cortés, Ó.; Martínez, G.; Rubio, N.; Blanco, J.; Santamaría, J.; Cascante, A.; Borrós, S. SPIONs' Enhancer Effect on Cell Transfection: An Unexpected Advantage for an Improved Gene Delivery System. *ACS Omega* **2019**, *4* (2), 2728−2740.
(21) Rohiwal, S. S.; Dvorakova, N.; Klima, J.; Vaskovicova, M.; Senigl, F.; Slouf, M.; Pavlova, E.; Stepanek, P.; Babuka, D.; Benes, H.; et al. Polyethylenimine Based Magnetic Nanoparticles Mediated Non-viral CRISPR/Cas9 System for Genome Editing. *Sci. Rep.* **2020**, *10* (1), 4619.
(22) Cruz-Acuña, M.; Halman, J. R.; Afonin, K. A.; Dobson, J.; Rinaldi, C. Magnetic Nanoparticles Loaded with Functional RNA Nanoparticles. *Nanoscale* **2018**, *10* (37), 17761−17770.
(23) Almeida, A. F.; Vinhas, A.; Gonçalves, A. I.; Miranda, M. S.; Rodrigues, M. T.; Gomes, M. E. Magnetic Triggers in Biomedical Applications − Prospects for Contact Free Cell Sensing and Guidance. *J. Mater. Chem. B* **2021**, *9* (5), 1259−1271.
(24) Amiri, A.; Bagherifar, R.; Ansari Dezfouli, E.; Kiaie, S. H.; Jafari, R.; Ramezani, R. Exosomes as Bio-inspired Nanocarriers for RNA Delivery: Preparation and Applications. *Journal of Translational Medicine* **2022**, *20* (1), 125.
(25) Aslan, C.; Kiaie, S. H.; Zolbanin, N. M.; Lotfinejad, P.; Ramezani, R.; Kashanchi, F.; Jafari, R. Exosomes for mRNA Delivery: A Novel Biotherapeutic Strategy with Hurdles and Hope. *BMC Biotechnology* **2021**, *21* (1), 20.
(26) Zu, H.; Gao, D. Non-viral Vectors in Gene Therapy: Recent Development, Challenges, and Prospects. *AAPS journal* **2021**, *23* (4), 78.
(27) Durymanov, M.; Reineke, J., Non-viral Delivery of Nucleic Acids: Insight Into Mechanisms of Overcoming Intracellular Barriers. *Frontiers in Pharmacology* **2018**, *9*, DOI: 10.3389/fphar.2018.00971.
(28) Zhang, S.; Sun, H.; Kong, W.; Zhang, B. Functional Role of microRNA-500a-3P-loaded Liposomes in the Treatment of Cisplatin-induced AKI. *IET Nanobiotechnology* **2020**, *14* (6), 465−469.
(29) Yan, Y.; Liu, X. Y.; Lu, A.; Wang, X. Y.; Jiang, L. X.; Wang, J. C. Non-viral Vectors for RNA delivery. *Journal of controlled release: official journal of the Controlled Release Society* **2022**, *342*, 241−279.
(30) Snyder, S. L.; Sobocinski, P. Z. An improved 2,4,6-trinitrobenzenesulfonic Acid Method for the Determination of Amines. *Anal. Biochem.* **1975**, *64* (1), 284−288.
(31) Taylor, S. C.; Nadeau, K.; Abbasi, M.; Lachance, C.; Nguyen, M.; Fenrich, J. The Ultimate qPCR Experiment: Producing Publication Quality, Reproducible Data the First Time. *Trends Biotechnol.* **2019**, *37* (7), 761−774.
(32) Hao, F.; Li, Y.; Zhu, J.; Sun, J.; Marshall, B.; Lee, R. J.; Teng, L.; Yang, Z.; Xie, J. Polyethylenimine-based Formulations for Delivery of Oligonucleotides. *Curr. Med. Chem.* **2019**, *26* (13), 2264−2284.
(33) Boussif, O.; Lezoualc'h, F.; Zanta, M. A.; Mergny, M. D.; Scherman, D.; Demeneix, B.; Behr, J. P. A Versatile Vector for Gene and Oligonucleotide Transfer Into Cells in Culture and In Vivo: Polyethylenimine. *Proc. Natl. Acad. Sci. U.S.A.* **1995**, *92* (16), 7297−301.
(34) Shim, B.-S.; Park, S.-M.; Quan, J.-S.; Jere, D.; Chu, H.; Song, M. K.; Kim, D. W.; Jang, Y.-S.; Yang, M.-S.; Han, S. H.; et al. Intranasal Immunization with Plasmid DNA Encoding Spike Protein of SARS-coronavirus/polyethylenimine Nanoparticles Elicits Antigen-specific Humoral and Cellular Immune Responses. *BMC Immunology* **2010**, *11* (1), 65.
(35) Sheppard, N. C.; Brinckmann, S. A.; Gartlan, K. H.; Puthia, M.; Svanborg, C.; Krashias, G.; Eisenbarth, S. C.; Flavell, R. A.; Sattentau, Q. J.; Wegmann, F. Polyethyleneimine is a Potent Systemic Adjuvant for Glycoprotein Antigens. *Int. Immunol.* **2014**, *26* (10), 531−538.
(36) Ortega-Muñoz, M.; Plesselova, S.; Delgado, A. V.; Santoyo-Gonzalez, F.; Salto-Gonzalez, R.; Giron-Gonzalez, M. D.; Iglesias, G. R.; López-Jaramillo, F. J. Poly(ethylene-imine)-Functionalized Magnetite Nanoparticles Derivatized with Folic Acid: Heating and Targeting Properties. *Polymers* **2021**, *13* (10), 1599.
(37) Nguyen, L. T.; Atobe, K.; Barichello, J. M.; Ishida, T.; Kiwada, H. Complex Formation with Plasmid DNA Increases the Cytotoxicity of Cationic Liposomes. *Biological & pharmaceutical bulletin* **2007**, *30* (4), 751−7.
(38) Bhattarai, S. R.; Kim, S. Y.; Jang, K. Y.; Lee, K. C.; Yi, H. K.; Lee, D. Y.; Kim, H. Y.; Hwang, P. H. Laboratory Formulated Magnetic Nanoparticles for Enhancement of Viral Gene Expression in Suspension Cell Line. *Journal of Virological Methods* **2008**, *147* (2), 213−218.
(39) Plank, C.; Rosenecker, J. Magnetofection: The Use of Magnetic Nanoparticles for Nucleic Acid Delivery. *Cold Spring Harbor Protocols* **2009**, *2009* (6), pdb.prot5230.
(40) Rueda-Gensini, L.; Cifuentes, J.; Castellanos, M. C.; Puentes, P. R.; Serna, J. A.; Muñoz-Camargo, C.; Cruz, J. C. Tailoring Iron Oxide Nanoparticles for Efficient Cellular Internalization and Endosomal Escape. *Nanomaterials* **2020**, *10* (9), 1816.
(41) Kamau Chapman, S. W.; Hassa, P. O.; Koch-Schneidemann, S.; von Rechenberg, B.; Hofmann-Amtenbrink, M.; Steitz, B.; Petri-Fink, A.; Hofmann, H.; Hottiger, M. O. Application of Pulsed-magnetic Field Enhances Non-viral Gene Delivery in Primary Cells from Different Origins. *J. Magn. Magn. Mater.* **2008**, *320* (8), 1517−1527.
(42) Pickard, M.; Chari, D. Enhancement of Magnetic Nanoparticle-mediated Gene Transfer to Astrocytes by 'Magnetofection': Effects of Static and Oscillating Fields. *Nanomedicine (London, England)* **2010**, *5* (2), 217−32.
(43) Yapici, M. K.; Al Nabulsi, A.; Rizk, N.; Boularaoui, S. M.; Christoforou, N.; Lee, S. Alternating Magnetic Field Plate for

https://doi.org/10.1021/acsami.2c22505
ACS Appl. Mater. Interfaces XXXX, XXX, XXX−XXX

Enhanced Magnetofection of Iron Oxide Nanoparticle Conjugated Nucleic Acids. *J. Magn. Magn. Mater.* **2019**, *469*, 598−605.
(44) Fouriki, A.; Farrow, N.; Clements, M. A.; Dobson, J. Evaluation of the Magnetic Field Requirements for Nanomagnetic Gene Transfection. *Nano Rev.* **2010**, *1*, 5167.
(45) Diener, C.; Keller, A.; Meese, E. Emerging Concepts of miRNA Therapeutics: from Cells to Clinic. *Trends in Genetics* **2022**, *38* (6), 613−626.
(46) Viola, A.; Munari, F.; Sánchez-Rodríguez, R.; Scolaro, T.; Castegna, A., The Metabolic Signature of Macrophage Responses. *Frontiers in Immunology* **2019**, *10*, DOI: 10.3389/fimmu.2019.01462.
(47) Abuawad, A.; Mbadugha, C.; Ghaemmaghami, A. M.; Kim, D.-H. Metabolic Characterisation of THP-1 Macrophage Polarisation using LC−MS-based Metabolite Profiling. *Metabolomics* **2020**, *16* (3), 33.
(48) Rostam, H. M.; Reynolds, P. M.; Singh, S.; Alexander, M. R.; Gadegaard, N.; Ghaemmaghami, A. Image Based Machine Learning for Identification of M1 and M2Macrophages. *J. Immunol.* **2016**, *196* (1 Supplement), 126.25.
(49) Luzina, I. G.; Keegan, A. D.; Heller, N. M.; Rook, G. A.; Shea-Donohue, T.; Atamas, S. P. Regulation of Inflammation by Interleukin-4: A Review of "Alternatives". *Journal of leukocyte biology* **2012**, *92* (4), 753−64.
(50) McCoy, C. E.; Sheedy, F. J.; Qualls, J. E.; Doyle, S. L.; Quinn, S. R.; Murray, P. J.; O'Neill, L. A. IL-10 Inhibits miR-155 Induction by Toll-like Receptors. *J. Biol. Chem.* **2010**, *285* (27), 20492−8.
(51) Makita, N.; Hizukuri, Y.; Yamashiro, K.; Murakawa, M.; Hayashi, Y. IL-10 Enhances the Phenotype of M2Macrophages Induced by IL-4 and Confers the Ability to Increase Eosinophil Migration. *Int. Immunol.* **2015**, *27* (3), 131−41.
(52) Mulens-Arias, V.; Rojas, J. M.; Pérez-Yagüe, S.; Morales, M. P.; Barber, D. F. Polyethylenimine-coated SPIONs Trigger Macrophage Activation through TLR-4 Signaling and ROS Production and Modulate Podosome Dynamics. *Biomaterials* **2015**, *52*, 494−506.
(53) Wu, J.; Zhu, J.; Wu, Q.; An, Y.; Wang, K.; Xuan, T.; Zhang, J.; Song, W.; He, H.; Song, L.; Zheng, J.; Xiao, J. Mussel-Inspired Surface Immobilization of Heparin on Magnetic Nanoparticles for Enhanced Wound Repair via Sustained Release of a Growth Factor and M2Macrophage Polarization. *ACS Appl. Mater. Interfaces* **2021**, *13* (2), 2230−2244.
(54) Lacey, D. C.; Achuthan, A.; Fleetwood, A. J.; Dinh, H.; Roiniotis, J.; Scholz, G. M.; Chang, M. W.; Beckman, S. K.; Cook, A. D.; Hamilton, J. A. Defining GM-CSF- and macrophage-CSF-dependent macrophage responses by in vitro models. *Journal of immunology (Baltimore, Md.: 1950)* **2012**, *188* (11), 5752−65.
(55) Argyle, D.; Kitamura, T. Targeting Macrophage-Recruiting Chemokines as a Novel Therapeutic Strategy to Prevent the Progression of Solid Tumors. *Front Immunol* **2018**, *9*, 2629.
(56) Liu, Y.; Cai, Y.; Liu, L.; Wu, Y.; Xiong, X. Crucial biological functions of CCL7 in cancer. *PeerJ.* **2018**, *6*, No. e4928.
(57) Ford, J.; Hughson, A.; Lim, K.; Bardina, S. V.; Lu, W.; Charo, I. F.; Lim, J. K.; Fowell, D. J. CCL7 Is a Negative Regulator of Cutaneous Inflammation Following Leishmania major Infection. *Front Immunol* **2019**, *9*, 3063.

https://doi.org/10.1021/acsami.2c22505
ACS Appl. Mater. Interfaces XXXX, XXX, XXX−XXX